論 文

大 韓 造 船 學 會 論 文 集
第 30 卷 第 1 號 1993 年 2 月
Transactions of the Society of
Naval Architects of Korea
Vol. 30, No.1, February 1993

수직원통 주위의 자유표면 층류운동의 수치해석

윤범상*, 김윤호**

Numerical Simulation of Laminar Flows for a Circular Cylinder Vertically Piercing Free Surface

by

Bum-Sang Yoon* and Yoon-Ho Kim**

요 약

본 논문에서는 점성유동에 미치는 자유표면의 영향을 조사하기 위하여 자유표면을 수직으로 관통하는 원통 주위의 유동을 수치 시뮬레이션 하였다. 수치해석 방법으로서 Artificial Compressibility Method 를 사용하였으며, 계산은 낮은 레이놀드수의 영역에 국한하였다. 계산결과는 자유표면에 가까운 유체영역에서 유선, 점성항력 등에 적지않은 영향이 있음을 보여주고 있다. 자유표면의 존재는 물체 후류 중의 와류를 물체로 부터 분리시키는 방향으로, 점성항력을 감소시키는 방향으로 작용하는 것으로 보인다.

Abstract

In this paper, effects of free surface on viscous flow is investigated.

Continuity equation coupled with Navier-Stokes equations are solved numerically by using an artificial compressibility method[1, 2]. The body-fitted generalized curvilinear coordinate system is employed to deal with arbitrary body shape. The IAF scheme with finite difference method is used to solve the equations, and a diagonal algorithm is applied to time-varying Jacobian matrices for the computational economics. Free surface shape is obtained by applying zero pressure condition to still water surface at each time step. A numerical test is made for larminar flow around a circular cylinder vertically piercing the free surface.

Computed flow patterns are largely affected by the existance of free surface in low Reynolds number flows treated in this paper. Free surface causes viscous pressure drag to vary much in depth direction in accordance with the variations of flow pattern.

접수일자 : 1992년 2월 20일, 재접수일자 : 1992년 8월 19일
* 정회원, 울산대학교 조선 및 해양공학과
** 정회원, 미국해군연구소

INTRODUCTION

Flow phenomena with the free surface may largely differ from those in an unbounded fluid. Free surface problem has been recognized as one of the most important themes in the field of hydrodynamics and numerous studies have perfo-rmed so far. Though, because of the difficulties, the flow is generally assumed inviscid and irrotational, quite good results could be obtained for various problems including linear and nonlinear waves, wave forces, and floating body motion.

However, in recent years, necessity of knowledge about specific local flow characteristics becomes more pronounced than ever and the introduction of fluid viscosity is now being recognized inevitable. For example, an analysis of ship stern flow, ship maneuvarability, ship viscous drag, wave-body impact and splash may be included in this unsolved problem category.

As the first step for developing a general algorithm to solve these free surface viscous flow problems, the flow around a circular cylinder pierrcing the free surface is simulated numerically in very low Reynolds numbers : 40,200 and 1000. The effects of the free surface on viscous flow is analyzed carefully by investigating the flow chracteristics including change of vortex shape and its size, flow separation, pressure and drag distribution along the vertical wall of the cylinder, configuration of the free surface.

Difficulty of solving the free surface problem stems from the fact that free surface shape is unkown on which boundary condition must be applied. This difficulty is usually eliminated by linearization of free surface conditions on the assumption that waves are infinitesimal and flow is inviscid and irrotational where Bernoulli's equation exists. However, for flows with large amplitude waves or complex free surface shape such as at the vicinity of a free surface piercing bodies, the linearization may not be applicable.

To avoid this difficulty, a fully Lagrangian or updated Lagrangian approach may be possible, where the free surface shape of zero pressure is tracked continuously in time domain[3, 4]. Alternatively, for problems with highly nonlinear shape of free surface, ALE(Arbitrary Lagrangian Eulerian) method may also be applicable, in which the fluid motions and mesh positions are treated separately[5]. Hino[6] obtained numerical solution of free surface viscous flow around ship hull by SUMMAC method[7], employing special meshes above the still water surface level to trace time-varying free surface configuration. Since they solve the unsteady problems, special technique must be developed to extend their approach to the steady problems like one treated here. Otherwise the computing time may be prohibitedly long to satisfy CFL condition because their numerical scheme in time is explicit or partly implicit. Furthermore their solution may not be guaranted to converge to the true solution as the case may be.

In this paper, steady state free surface shape is obtained by applying zero pressure condition to the still water surface level at each time step. This approximate procedure is very effective in solving steady free surface problems by time-marching algorithm with Eulerian meshes. Primitive variables, namely pressure and velocities, are solved directly from the continuity equation coupled with Navier-Stokes equations with appropriate initial and boundary conditions. Basic theory used here is an artificial compressibility method, which was first proposed by Chorin[1, 2]. The use of artificial compressibility results in a system of hyperbolic-type equations of motion. Waves of finite speed are introduced into the incompressible flow field as a medium to distribute pressure. By introducing artificial compressibility, major difficulty in developing time marching procedure caused from absence of pressure term in continuity equation can be overcome. The solution obtained by using the present method converges to the incompressible limit and the effect of the artificial compressibility vanishes when the steady state is reached. The validity and the effectiveness of this method are proven by some authors through their works about

an unbounded fluid flow problems without free surface[8, 9]. For convenience and flexibility, generalized curvilinear coordinates is chosen in derivation of equations. The numerical algorithm used to advance governing equations in time is non-iterative, implicit, approximately factored, finite difference scheme[10]. Moreover, for the computational economics, diagonalization algorithm[12, 13, 14] is applied to the time-varying Jacobian matrices involved in implicit terms of delta form of finite difference equations.

A circular cylinder vertically piercing the free surface is selected as a test problem and computed results are presented to verify the theory.

NUMERICAL SCHEME

Governing Equations

By introducing an artificial compressibility parameter β, the continuity equation is modified by adding a time derivative of the pressure term and becomes:

$$\frac{1}{\beta}\frac{\partial p}{\partial t}+\frac{\partial u_i}{\partial x_i}=0 \tag{1}$$

Dimensionless Navier-Stokes equations are written in conservation form as follows:

$$\frac{\partial u_i}{\partial t}+\frac{\partial u_i u_j}{\partial x_i}=-\frac{\partial p}{\partial x_i}-f_i+\frac{\partial \tau_{ij}}{\partial x_j} \tag{2}$$

where

$$f_i=\begin{cases}0 & \text{for } i=1,\ 2\\ \dfrac{1}{Fn^2} & \text{for } i=3\end{cases}$$

$$\tau_{ij}=\frac{2}{Re}S_{ij}-R_{ij}$$

$$S_{ij}=\frac{1}{2}\left(\frac{\partial u_i}{\partial x_j}+\frac{\partial u_j}{\partial x_i}\right)$$

Here, S_{ij} is the strain rate tensor, R_{ij} are the Reynolds stresses, and f_3 the gravitational force. Various levels of closure models for R_{ij} are possible, but is not taken into consideration in this paper.

As shown in Fig.1, $x_i(x,y,z)$ are Cartesian coordinates normalized by cylinder diameter D_c where x is the free stream direction, y the lateral direction, and z the vertical direction in positive upward. $u_i(u,v,w)$ are velocity components normalized by uniform flow U_0. t is time normalized by $\frac{D_c}{U_0}$ and p is pressure normalized by ρU_0^2, where ρ is the fluid density. Re and Fn are Reynolds number and Froude number respectively based on the U_0 and D_c.

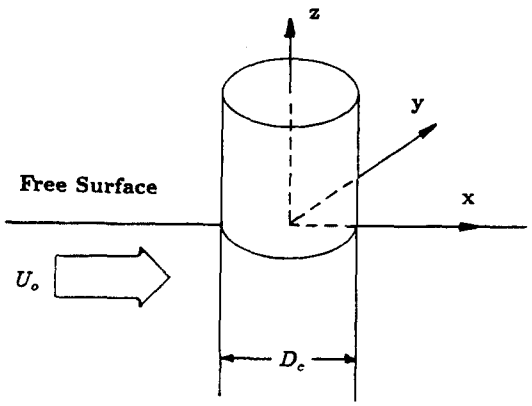

Fig.1 Coordinate system

Following Hino[6], ϕ is the pressure from which hydrostatic component is subtracted, i.e.,

$$\phi=p+\frac{z}{Fn^2} \tag{3}$$

To perform calculations of 3-dimensional arbitrary shaped geometries, the physical coordinates are transformed into general curvilinear coordinates by introducing the following independent variables:

$$\tau=t$$
$$\xi=\xi_1=\xi(x,y,z)$$
$$\eta=\xi_2=\eta(x,y,z)$$
$$\zeta=\xi_3=\zeta(x,y,z)$$

After transformation, combining the governing equations (1) and (2) yield the following equation:

$$\frac{\partial \hat{D}}{\partial \tau}+\frac{\partial}{\partial \xi_i}(\hat{E}_i-\hat{E}_{vi})=0 \tag{4}$$

where

$$\hat{D} = \frac{1}{J}D,\ \hat{E}_i = \frac{1}{J}E_i,\ \hat{E}_{vi} = \frac{1}{J}E_{vi}$$

and

$$D = [\phi, u, v, w]^T \tag{5}$$

$$E_i = \begin{bmatrix} \beta U_i \\ uU_i + (\xi_i)_x\phi \\ vU_i + (\xi_i)_y\phi \\ wU_i + (\xi_i)_z\phi \end{bmatrix} \tag{6}$$

The viscous terms are given by :

$$E_{vi} = \frac{1}{Re}\left(\frac{\partial \xi_i}{\partial x_j}\frac{\partial \xi_k}{\partial x_j}\frac{\partial}{\partial \xi_k}\begin{bmatrix} 0 \\ u \\ v \\ w \end{bmatrix} + \frac{\partial \xi_i}{\partial x_j}\frac{\partial u_j}{\partial \xi_k}\begin{bmatrix} 0 \\ \frac{\partial \xi_k}{\partial x} \\ \frac{\partial \xi_k}{\partial y} \\ \frac{\partial \xi_k}{\partial z} \end{bmatrix}\right) \tag{7}$$

Here the Jacobian of the transformation is defined as :

$$J = det\frac{\partial(\xi,\eta,\zeta)}{\partial(x,y,z)} = \begin{vmatrix} \xi_x & \xi_y & \xi_z \\ \eta_x & \eta_y & \eta_z \\ \zeta_x & \zeta_y & \zeta_z \end{vmatrix} \tag{8}$$

and U_i are the contravariant velocities :

$$U_i = \frac{\partial \xi_i}{\partial x_j}u_j \tag{9}$$

Numerical Algorithm

Application of Impicit Approximate Factorization algorithm introduced by Beam and Warming[10] results in the following time-marching difference equation of delta from :

$$L_\xi L_\eta L_\zeta(D^{n+1} - D^n) = RHS \tag{10}$$

where

$$L_{\xi_i} = I + \frac{\Delta\tau}{2}J\delta_{\xi_i}(A_i^n - \Gamma_i) + \varepsilon_{imp} \tag{11}$$

$$RHS = -\Delta\tau\delta_{\xi_i}(E_i - E_{vi})^n - \varepsilon_{exp} \tag{12}$$

Here, $\delta_{\xi i}$ is central difference operator in ξ_i direction, and I is the 4×4 identity matrix. Implicit and explicit numerical smoothing terms, which are ε_{imp} and ε_{exp} respectively, are introduced to stabiliz e the calculation. Superscripts n, $n+1$ implicate time steps. Taylor series expansion of unknown D about n time step gives the Jacobian matrices which relates the unknowns of the two neighboring time steps as the following :

$$A_i = \frac{1}{J}\begin{bmatrix} 0 & L_{i1}\beta & L_{i2}\beta & L_{i3}\beta \\ L_{i1} & Q_i + L_{i1}u & L_{i2}u & L_{i3}u \\ L_{i2} & L_{i1}v & Q_i + L_{i2}v & L_{i3}v \\ L_{i3} & L_{i1}w & L_{i2}w & Q_i + L_{i3}w \end{bmatrix} \tag{13}$$

Similarly, difference operators of viscous terms in implicit side are written as :

$$\Gamma_i = \frac{1}{Re}\frac{1}{J}(L_{ij}L_{kj}\delta_{\xi_k}I_1 + \Omega_i) \tag{14}$$

in which

$$Q_i = L_{ij}u_j \tag{15}$$

$$L_{ij} = \frac{\partial \xi_i}{\partial x_j} \tag{16}$$

$$I_1 = \begin{bmatrix} 0 & 0 & 0 & 0 \\ 0 & 1 & 0 & 0 \\ 0 & 0 & 1 & 0 \\ 0 & 0 & 0 & 1 \end{bmatrix} \tag{17}$$

$$\Omega_i = \begin{bmatrix} 0 & 0 & 0 & 0 \\ 0 & \Omega_{i11} & \Omega_{i12} & \Omega_{i13} \\ 0 & \Omega_{i21} & \Omega_{i22} & \Omega_{i23} \\ 0 & \Omega_{i31} & \Omega_{i32} & \Omega_{i33} \end{bmatrix} \tag{18}$$

where

$$\Omega_{ijk} = L_{ik}L_{lj}\delta_{\xi_l} \tag{19}$$

If orthogonal grid is used for laminar flow like that employed in the present calculation, see Fig.2, equation (14) can be simplified as follows :

$$\Gamma_i = \frac{1}{Re}\frac{1}{J}L_{ij}L_{ij}\delta_{\xi_i}I_1 \tag{20}$$

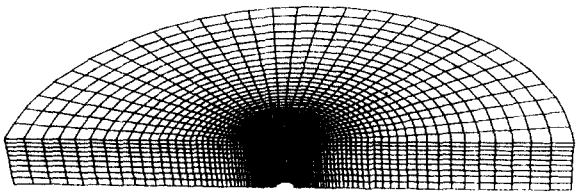

Fig.2 Perspective view of o-grid around a body

In factoring the finite difference equations to obtain eq.(10), the equation unavoidably involves the cross differencing error. In order to maintain the second-order accuracy of the differencing scheme, the factorization error must be kept smaller everywhere in the computational domain than the original terms in the equations. Proper choice of artificial compressibility parameter β is thus very important since the Jacobians A_i contain β, and Kwak et al[11] provided upper and lower bounds for β. In this paper, $\beta=5$ is chosen throughout all the calculations. Furthermore, by the use of a similarity transformation [12, 13, 14] which diagonalize the Jacobian matrices A_i, solutions may be obtained by solving scalar tridiagonal matrices instead of solving block diagonal matrices. Detailed procedures of diagonalization including derivation of transformation matrices are discussed in Reference[14]

Boundary Conditions

Once the numerical algorithm has been developed, the next most important procedure is the proper implementation of the boundary conditions. No-slip, no-penetration condition and condition of zero normal gradient for pressure are applied on the body surface, $\frac{\partial p}{\partial n}=0$. Because of the symmetry of the problem about $y=0$, $v=0$ on the plane of symmetry. The bottom is truncated into finite one and extrapolated values for ϕ, u, v, and w are applied from values of the two neighboring planes vertical to the ζ-direction. On the inflow boundary, flow velocity is uniform in x-direction and p hydrostatic pressure with zero wave elevation. On the outflow boundary, the values of ϕ, u, v, and w are extrapolated first using the values of two neighboring planes, and linear correction is added at each time step to satisfy the condition of mass and momentum conservation in the solution region. It is verified by Chang et al[15] that instabilities are not introduced into the flow field by performing this correction.

On the free surface, the following approximate dynamic condition is applied at every moment:

$$\phi = -\frac{\zeta}{Fn^2} \text{ on } z=0 \tag{21}$$

During computation, the dynamic free surface condition is applied to the still water surface approximately and the unknown variables on the surface are extrapolated from the two neighboring planes. Resultant free surface shape ζ is obtained form Equation(20) after enough convergence is achieved. This process proved, though approximate, to be effective when time-marching is carried out with Eulerian meshes.

NUMERICAL RESULTS AND DISCUSSION

Computational grid points are clustered near the body and near the free surface as shown in Fig. 2. The number of grid points are 52, 32 and 10 in the ξ, η and ζ direction, respectively, and algebraic method[16] is used to determine their coordinates. Computation is carried out for the flows of three different Reynolds numbers: 40, 200 and 1000.

Convergence histories are given in Fig.3(A) and 3(B). Time variation of average absolute value of velocity divergence at each node is shown is Fig. 3(A) as a mean for showing how the incompressible limit is achieved. Fig.3(B), which is time history of average variation of root mean square values for the 4 variables ϕ, u, v, and w, shows a way to the steady state limit. For a typical example of converged sulution, velocity profiles near the cylinder surface in case of Re=200, 2-dimensional case without free surface, is shown in Fig.4.

Free Surface Affection Layer

Numerical results show how the viscous flow patterns are affected by the existence of the free surface, the effects is significant in a layer attached to the free surface, and we call it free sur-

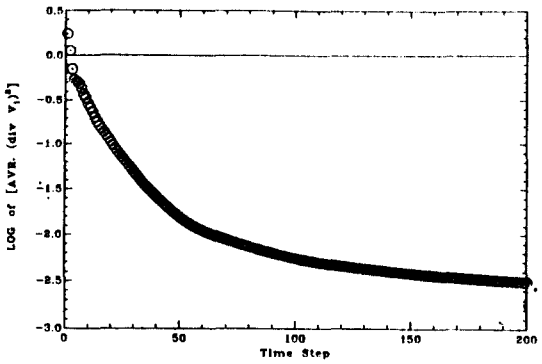

Fig.3(A) Convergence history to the incompressible limit
(Re=200, Fn=0.5000, No.of Mesh=52×32×10)

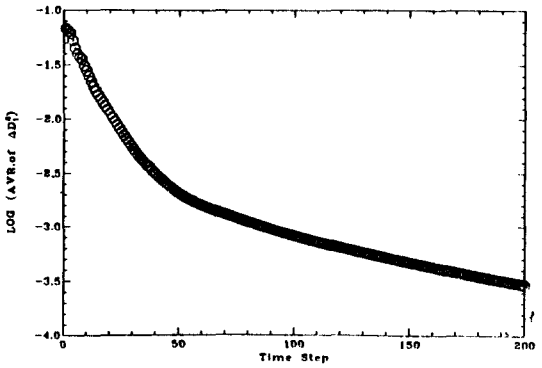

Fig.3(B) Convergence history to the steady state
(Re=200, Fn=0.5000, No.of Mesh=52×32×10)

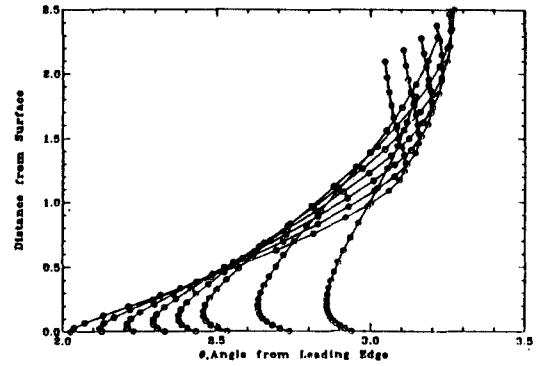

Fig.4 Velocity Profile around Circular Cylinder
(Re=200., Time=10.0000sec)

face affection layer. Simulated stream lines on the planes of various vertical locations are compared with 2-dimensional results without free surface in Fig.5(A,B,C), which are for Re=40, 200 and 1000, respectively.

Free surface affection layer consists of two parts, where flow phenomena is thought to be quite different. —upper layer and lower layer— In the upper layer, vortex is detached from the body. The distance between the detached vortex and the body increases as the depth increases until the

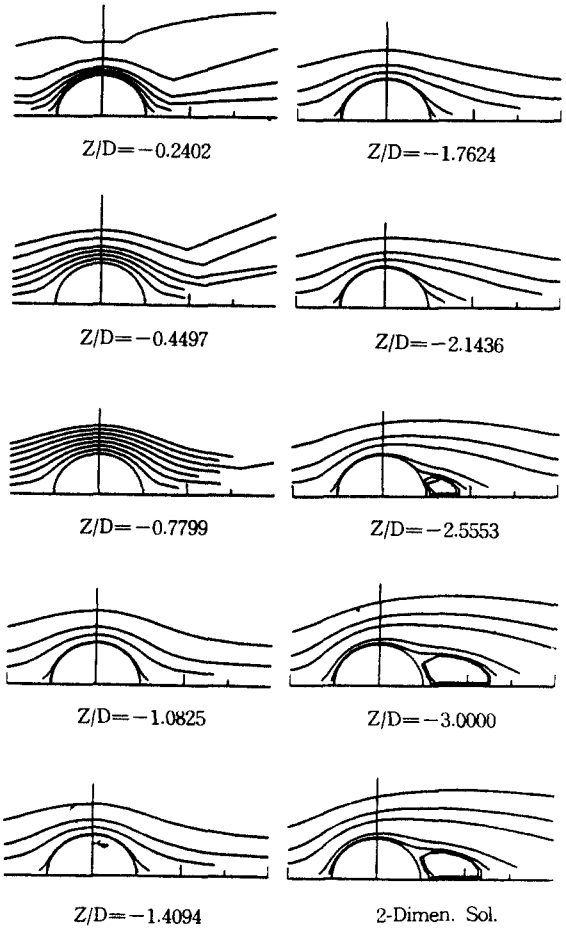

Fig.5(A) Stream lines around circular sections at various vertical locations(Re=40)

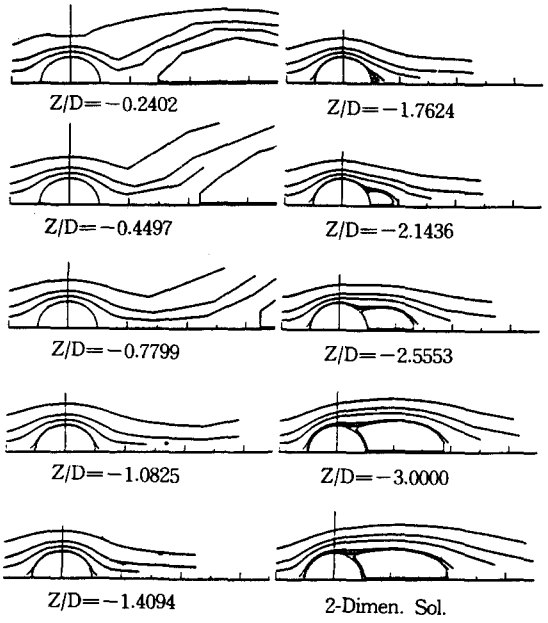

Fig.5(B) Stream lines around circular sections at various vertical locations(Re=200)

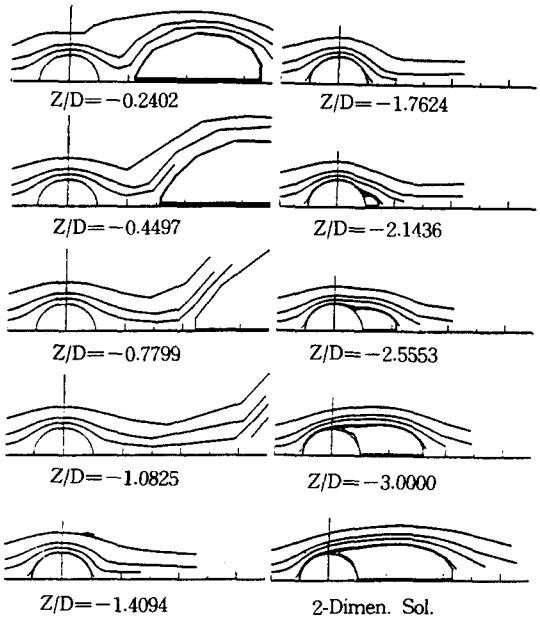

Fig.5(C) Stream lines around circular sections at various vertical locations(Re=1000)

outer limit of this layer being arrived. In the lower layer, newly generated vortex grows as the depth increases to the steady limit at this layer ends. Therefore, at first glance, stream lines near the critical depth where the lower limit of the upper layer and the upper limit of the lower layer meet seem to be very similar to those for an ideal flow because the detached vortex goes to infinity and separation does not occur. But there exists much difference between them in the flow region very close to the body surface, well known as body boundary layer which is not shown in these figures. In laminar flow, thickness of the free surface affection layer increases with increase of Reynolds number as shown in Fig.5.

Free Surface Effect on Viscous Pressure Drag

Fig.6 indicates effects of free surface on the viscous pressure drag acting on the various sections of the cylinder. In the upper part of the free surface affection layer, change of pressure drag is mainly caused by detached vortex and it decreases as the sectional position from the free surface increases. In the vicinity of the transition point, which is lower extreme of the upper layer the drag approaches to the minimum value because the drag is only caused by the thin body boundary layer not accompanying any flow separation.

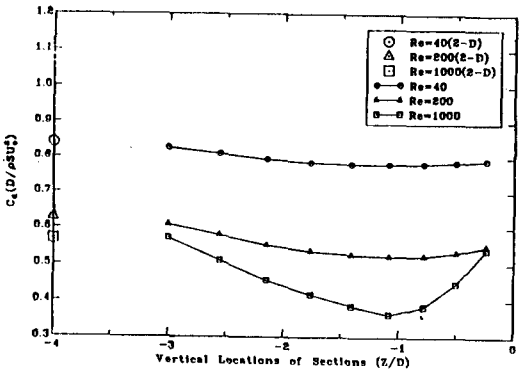

Fig.6 Free surface effects on viscous pressure drag (Fn=0.5000, No.of Mesh=52×32×10)

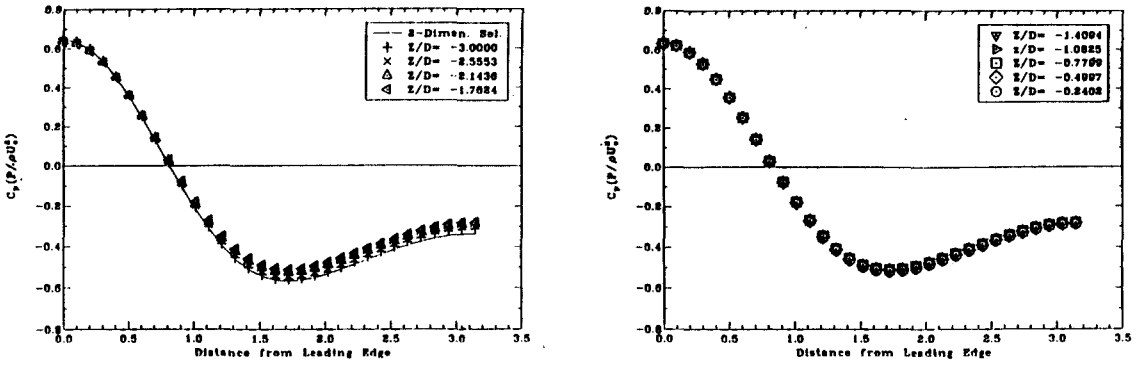

(A) (B)

Fig.7 Pressure distributions on circular sections at various vertical locations(Re=40)

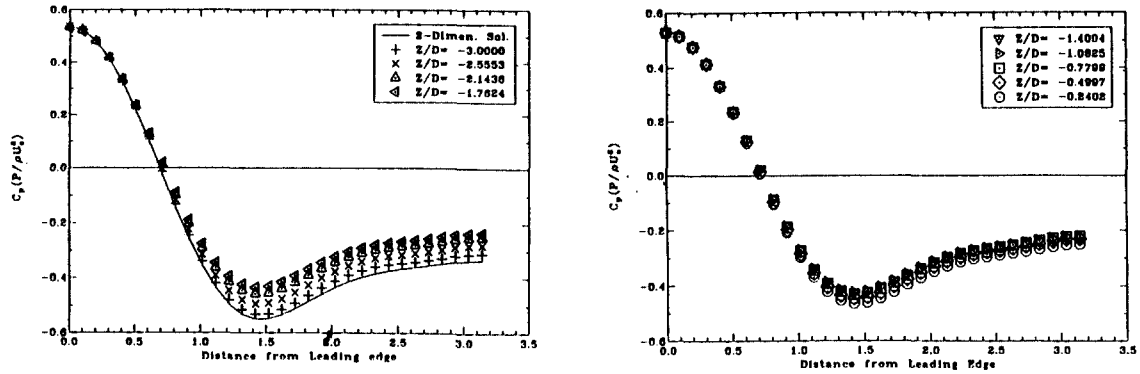

(A) (B)

Fig.8 Pressure distributions on circular sections at various vertical locations(Re=200)

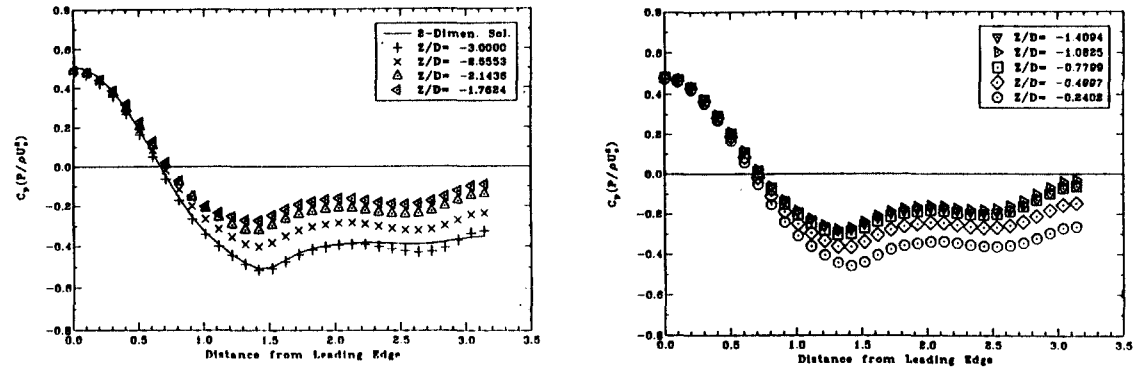

(A) (B)

Fig.9 Pressure distributions on circular sections at various vertical locations(Re=1000)

Beyond this point, it increases gradually and finally it reaches to the maximum value as the vortex grows to its steady maximum size, where the free surface effect vanishes. Generally speaking from the only numerical results, in the flow range of low Reynolds number, the larger the Reynolds number the larger the free surface effects on the viscous drag. For example, maximum about 35 percent of the drag is decreased compared to that of deep water at the transition layer in case of Re=1000. Similar discussions can also be said for viscous pressure distributions as shown in Fig.7, 8 and 9, which are for Re=40, 200 and 1000, respectively. Differencies in the sectional pressure distributions on the surface of afterbody are much larger than those on the forebody in accordance with the change of depth, which is similar to the fact that the variations of flow patterns affected by depths are more remarkable in down stream region than upstream region as shown in Fig.5. While, measured drag coefficients for an infinite circular cylinder are about 1.05, 0.85 and 0.50 for Re=40, 200 and 1000, respectively[17]

Since the main aim of this paper is to investigate the free surface effect on the viscous flow, viscous effect on the free surface or viscous effect in the wave drag are not treated here. Change in Froude number does not cause any variation of viscous pressure drag or flow pattern at all in the present calculation, though it makes much difference in the free surface shapes. To know the interaction between free surface and viscous flow more accurately, not only the primary effect of existence of the free surface but also its nolinear effects by an amount of free surface movement, which depends on Froude number, are to be investigated.

Free Surface Shapes

Free surface shapes are obtained by dynamic free surface condition of zero pressure on the still water surface level. And hence, their elevations are linearly dependent on the square of the Froude number as shown in Fig.10(B) and 10(C), which are 10 times magnified in vertical direction. From the Fig.10(A), 10(B) and 10(D), numerical results show that the larger the Reynolds number is,the larger the distortion of the free surface is resulted in.

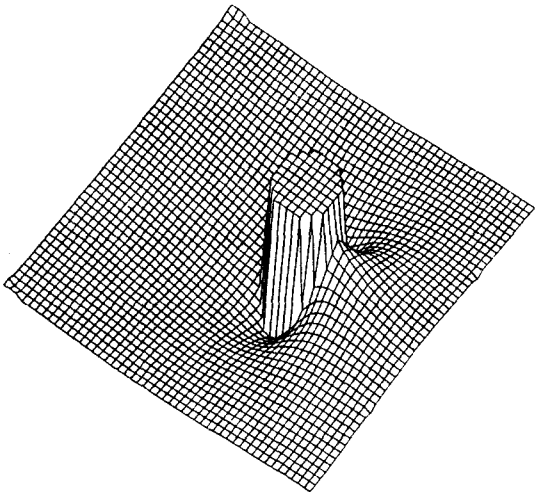

Fig.10(A) Computed water surface around circular cylinder for Re=40, Fn=0.5, Height is ten times magnified.

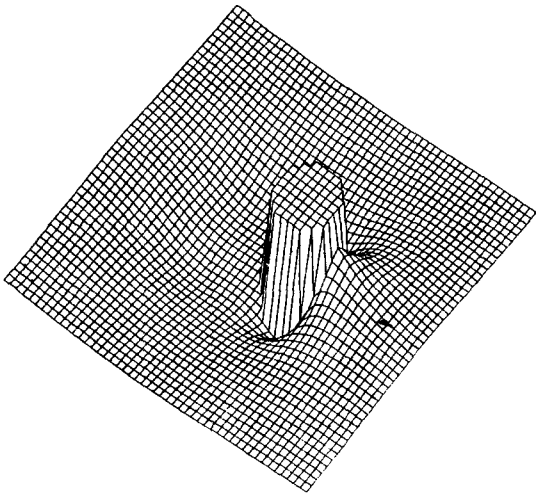

Fig.10(B) Computed water surface around circular cylinder for Re=200, Fn=0.5, Height is ten times magnified.

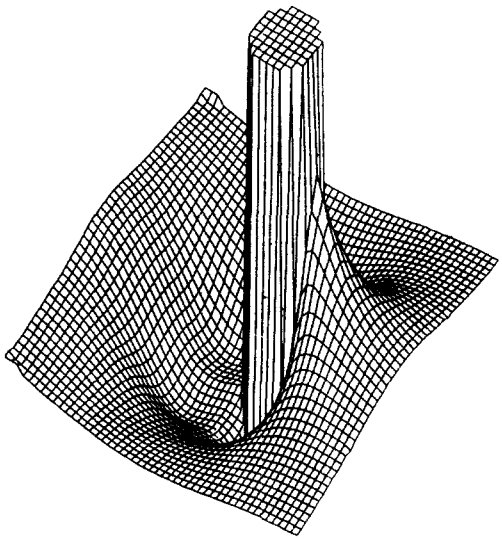

Fig.10(C) Computed water surface around circular cylinder for Re=200, Fn=1.0, Height is ten times magnified.

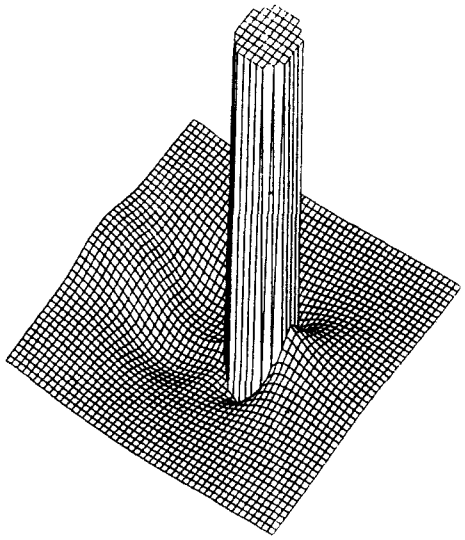

Fig.10(D) Computed water surface around circular cylinder for Re=1000, Fn=0.5, Height is ten times magnified.

All the calculated results are those at 200 time step. Computations are carried out using the VAX Micro Computer at Surface Ship Dynamics Branch, Carderock Division, Naval Surface Warfare Center. CPU time required to compute 1 step of 1 grid point is about 0.007 seconds. Since all the above discussions are exclusively based upon the computed results without comparing with measured values, the characteristics of viscous free surface flow explained here or the computational method used in this paper are to be verified through more detailed discussion and comparisons with other numerical and experimental results.

CONCLUDING REMARKS

Artificial compressibility method is applied to the steady, incompressible, viscous, laminar flow with free surface. Flow around a circular cylinder vertically piercing the free surface is simulated numerically, and the effects of free surface on the characteristics of viscous flow are investigated.

Flow field experiences large variation by existence of the free surface, that is, vortex is detached in the upper part of the free surface effection layer and newly generated vortex grows in the lower part of the layer. In the layer, viscous pressure, accordingly viscosity induced drag, are also influenced by the free surface. The drag decreases first until the minimum value is reached at transition position, and then it increases as the depth location approaches the free surface. The larger the Reynolds number is, the larger the free surface effects on the viscous flow characteristics in the region of low Reynolds number.

ACKNOWLEDGEMENTS

The authors express their gratitude to Dr.D.C. Kwak at NASA Ames Research Center who supplied them with INS3D code, becuase of which it was possible to develop a new version used in this work. They also wish to thank Mr.Geoffrey Cox, Mr.Jon Dalzell, Mr.Lewis Motter, Mr.Harry Jones and all the members at surface ship dynamics branch of CDNSWC who helped one of the authors to work under very comfortable condition. Special thanks are extended to Dr.William Morgan, Mr.Vincent Monacella and Dr.Young S.Hong who

made it possible for one of the two authors to do research at CDNSWC.

This research was supported by University of Ulsan.

REFERENCES

[1] A.J. Chorin, "A numerical methods for solving incompressible viscous flow problems", *Journ. Comput. Physics* 2,12-26(1967).

[2] A.J. Chorin, "Numerical solution of Navier-Stokes equations", *Journ. Math. Comput.* 22 (104), 745-762(1968).

[3] B. Ramaswamy and M. Kawahara, "Lagrangian finite element analysis applied to viscous free surface fluid flow", *Int. Journ. Numer. Methods in Fluids* 7(1987).

[4] B.S. Yoon, "Updated Lagrangian finite element analysis of water impact problem by the splitting method", *Proc. 10th Symp. Ocean Eng. SNAJ,* Tokyo, 133−141(1991).

[5] J. Donea et al, "An arbitrary Lagrangian Eulerian finite element method for transient dynamic fluid-structure interaction", *Comput. Methods in Applied Mech. and Eng.* 33, 689−701(1982).

[6] T. Hino, "Computation of a free surface flow around an advancing ship by the Navier-Stokes equations", *Proc. 5th Conf.Numer.Ship Hydro.,* Hiroshima, 103−115(1989).

[7] R.K.C. Chan and R.L. Street, "A computer study of finite amplitude water waves", *Journ. Comput. Physics* 6(1970).

[8] D. Kwak et al, "A three-dimensional incompressible Navier-Stokes flow solver using primitive variables", *AIAA* 24(3), 390−396(1986).

[9] C.I. Yang et al, "Numerical simulation of three dimensional viscous flow around a submergible body", *Proc. 5th Conf. Numer. Ship Hydro.* Hiroshima, 59−70(1989).

[10] R.M. Beam and R.F. Warming, "An implicit finite difference algorithm for hyperbolic systems in conservation law form", *Journ. Comput, Physics* 22, 87−110(1976).

[11] D.C. Kwak et al, "On the Accuracy of the pseudocompressibility method in solving the incompressible Navier-Stokes equations", *AIAA 18th Fluid Dynamics,* Plasmadynamics, Laser Conf., Cincinatti(1985).

[12] E. Turkel, "Symmetrization of the fluid dynamic matrices with applications", *Math. Comput.* 27, 729−736(1973).

[13] T.H. Pullian and D.S. Chaussee, "A diagonal form of an implicit approximate factorization algorithm", *Journ. Comput. Physics* 39, 347−363(1981).

[14] S.E. Rogers et al, "A diagonal algorithm for the method of pseudocompressibility", *AIAA-/ASME 4th Fluid Mechanics,* Plasma Dynamics and Lasers Conf., Atlanta(1986).

[15] J.L.C. Chang et al, "Numerical simulation methods of incompressible flows and an application to the space shuttle main engine", *Inter. Journ. Numer. Methods in Fluids* 8, 1241−1268(1988).

[16] P.R. Eiseman, "In numerical grid generation", ed. by J.F. Thompson(North Holland, Amsterdam), 193−234(1982).

[17] H. Schlichting, "Boundary layer theory", 6th ed., McGraw-Hill(1968).